

Prediction of Spin-Polarization Characteristics of Al-Doped Single-Walled SiC Nanotubes

V.N. JAFAROVA^a, A.A. HADIYEVA^{a,b} AND V.K. SARIJANOVA^a

^a*Azerbaijan State Oil and Industry University, 20 Azadliq Ave., AZ-1010 Baku, Azerbaijan*

^b*Khazar University, 41 Mehseti Str, AZ-1096 Baku, Azerbaijan*

Received: 24.08.2025 & Accepted: 09.10.2025

Doi: [10.12693/APhysPolA.148.177](https://doi.org/10.12693/APhysPolA.148.177)

*e-mail: aynura.hadiyeva@asoiu.edu.az

The present work explores how aluminum substitution affects the electronic, magnetic, and structural properties of single-walled (6,0) silicon carbide nanotubes, based on spin-polarized density functional theory simulations. The incorporation of Al atoms causes pronounced changes in the band structure, driving the system toward half-metallic behavior, where the spin-up channel retains semiconducting characteristics while the spin-down channel exhibits metallic conductivity. Analysis of the partial density of states demonstrates that states close to the Fermi energy primarily originate from the carbon *p* orbitals together with contributions from aluminum *d* orbitals. Spin-resolved charge density mapping indicates that a net magnetic moment of nearly $1.0 \mu_B$ is localized mainly on carbon atoms surrounding the dopant. Total energy comparisons between ferromagnetic and antiferromagnetic spin arrangements establish the antiferromagnetic configuration as the ground state. Collectively, these results highlight that Al-doped SiC nanotubes are strong candidates for spintronic applications, particularly in spin filters and antiferromagnetic memory devices, owing to their half-metallicity and robust magnetic ordering.

topics: aluminum-doped silicon carbide (Al-doped SiC), nanotube, ferromagnetic, half-metallic

1. Introduction

In recent years, two-dimensional (2D) semiconductor systems with graphene-like features have attracted strong research interest because of their distinctive structural, chemical, and electronic characteristics, making them promising for future spintronic and optoelectronic technologies [1, 2]. Among these systems, silicon carbide (SiC) stands out as a third-generation wide-band-gap material that combines high thermal conductivity, chemical durability, and mechanical stability with a large band gap. These qualities have enabled SiC to be employed in demanding environments, such as high-temperature, high-frequency, and high-power electronic devices [2–4]. Beyond electronics, SiC nanostructures have also been explored for biomedical sensing, biocompatibility, and energy-harvesting applications [5].

Previous theoretical and experimental investigations have shown that silicon carbide nanotubes (SiCNTs) exhibit more stable electronic and magnetic features compared to conventional carbon nanotubes (CNTs) [6–10]. To broaden the potential of 1D, 2D, and 3D Si-based nanostructures, considerable attention has been directed toward impurity doping as a strategy to tune their electronic and magnetic responses. In particular,

single-walled SiCNTs (SWSiCNTs) doped with metallic and transition-metal elements are predicted to be promising candidates for chemical sensing, hydrogen storage, and nanoscale spintronic applications. Such dopants often cause charge redistribution, and their *d*-orbital interactions can induce magnetic ordering within the SiCNT framework [11, 12]. For instance, Heidarzadeh [8] reported that cobalt doping of cubic SiC (3C-SiC) creates a metallic intermediate band within the band gap through the substitution of Co atoms in the crystal lattice. This intermediate band arises due to the interaction between the crystalline potential and the spin interaction of Co *d* orbitals, which enhances the photovoltaic conversion efficiency by enabling absorption of sub-band-gap photons [8]. Our previous studies showed that cobalt doping converts cubic SiC into a metallic state, while Au- and Co-doped (6,0) SiCNTs exhibits half-metallicity, making them promising candidates for spintronic device applications [13, 14]. Complementary density functional theory (DFT) studies have further confirmed that different SiCNT chiralities retain semiconducting band gaps, proving their flexibility for functional modifications [15].

Because silicon and carbon share comparable valence electron configurations, the formation of fullerene-like and tubular SiC structures, including the chiral (6,0) nanotube, has long been anticipated.

More recently, first-principles studies including approaches that integrate DFT with machine learning have shown that noble-metal-doped SiCNTs, such as Ag- and Au-doped systems, possess tunable magnetic properties desirable for spintronic device engineering [16–19].

Against this background, the present work focuses on aluminum as a group-III dopant. Al substitution in SiC nanotubes is of particular interest because it can significantly alter electronic and magnetic characteristics in ways that differ from transition-metal doping. Understanding these effects provides opportunities for the design of nanoscale devices with optimized spin-dependent performance and robust stability. The relatively limited prior studies on Al-doped SiCNTs underline the novelty of this research, which aims to clarify their role and broaden the knowledge about doping-induced modifications in SiC-based nanomaterials [20].

2. Computational methodology

In this work, spin-polarized first-principles calculations within the framework of density functional theory (DFT) were employed to examine the electronic and magnetic properties of aluminum-substituted single-walled silicon carbide nanotubes (SWSiCNTs) with a (6,0) zigzag geometry. A scalar-relativistic approximation was used throughout the calculations, incorporating mass-velocity and Darwin terms, while the spin-orbit coupling (SOC) effects were neglected due to the light atomic masses of Si, C, and Al, for which SOC is expected to have minimal impact on the electronic and magnetic properties of the system. The simulations were carried out using the Atomistix ToolKit (ATK) platform, which combines DFT with localized basis sets and a pseudopotential approach. For the treatment of exchange-correlation effects, the local spin density approximation (LSDA) was applied. Since conventional LSDA tends to underestimate band gaps, a Hubbard U correction (LSDA+ U) was introduced to better capture localized electronic states [19, 20]. Consistent with earlier theoretical studies, the on-site Coulomb parameters were set to $U_{\text{Si}} = 5.0$ eV for silicon $3d$ states and $U_{\text{C}} = 4.8$ eV for carbon $2p$ states in order to reproduce experimental band gap values of bulk SiC.

For the bulk three-dimensional (3D) SiC reference structure, a hexagonal crystal symmetry was considered. In contrast, for the nanotube calculations, a zigzag (6,0) single-walled SiC nanotube was modeled. Periodic boundary conditions were applied along the nanotube axis only, simulating an infinite one-dimensional (1D) system. No additional symmetry constraints were imposed beyond the intrinsic translational symmetry of the nanotube.

In the doped configuration, one silicon atom located near the center of the nanotube wall was substituted by an aluminum atom, corresponding to a substitutional doping concentration of $\approx 4.2\%$. This specific substitution site was selected to maintain the structural symmetry of the (6,0) SiCNT and to minimize edge effects in the periodic simulation. The simulation model was based on a periodic (6,0) SiCNT system containing 24 atoms per unit cell, with doping implemented through this single-atom substitution. After substitution, the structure was fully relaxed to allow the system to reach its ground-state geometry. Geometry optimization revealed slight local distortions in the vicinity of the Al dopant due to the difference in atomic radii between Al and Si, but no significant changes occurred in the overall structural integrity or periodicity of the nanotube. Geometry optimization was performed with a plane-wave energy cutoff of 100 Ry (equivalent to 50 Hartree), and the Brillouin zone was sampled using a $1 \times 1 \times 5$ Monkhorst-Pack k -point grid along the nanotube axis. The energy convergence criterion was set to 10^{-5} eV per atom between successive self-consistent field (SCF) iterations to ensure accurate and reliable results. Convergence thresholds were set to 0.001 eV/Å for atomic forces and 0.001 eV/Å³ for stress tensor components.

Spin-resolved electronic structures — including the density of states (DOS) and band structures — were computed to analyze the spin polarization and electronic transitions near the Fermi level. Mulliken population analysis was employed to evaluate the atomic magnetic moments and orbital contributions. Additionally, the spin-polarized charge density distribution was visualized to examine the spatial localization of magnetic moments induced by the Al dopant.

The valence electron configurations considered for the pseudopotentials were as follows:

- Si — [Ne] $3s^2 3p^2$,
- C — [He] $2s^2 2p^2$,
- Al — [Ne] $3s^3 3p^1$.

This computational framework provides a robust and accurate approach to exploring the spintronic potential of Al-doped SiC nanotube systems.

To determine the most stable spin configuration, both ferromagnetic (FM) and antiferromagnetic (AFM) states were examined.

3. Results and discussion

3.1. Electronic characteristics of SWSiC:Al nanotubes

Before investigating the nanostructure, we first studied the electronic properties of bulk SiC with a three-dimensional (3D) structure. By selecting an appropriate computational method, we successfully

calculated the band structure of this compound. The results obtained from our calculations are in good agreement with available experimental data.

Silicon carbide (SiC) in the wurtzite (2H) structure exhibits a wide indirect band gap of ≈ 3.3 eV, making it highly suitable for applications in electronics and optoelectronics. Several theoretical studies have explored the electronic properties of both bulk wurtzite SiC [21–23] and its nanostructures [24–30]. In [21], the authors reported electronic band structures and density of states (DOS) using DFT with the generalized gradient approximation (GGA) and the GW (where G refers to the Green’s function and W to the screened Coulomb interaction) correction scheme. They calculated a band gap of ≈ 3.17 eV for the hexagonal SiC structure. Sinelnik et al. [21] and Huang et al. [22] also investigated the electronic band structure of 2HSiC using the GGA method and obtained a band gap of 2.3 eV, which underestimates the experimental value by about 1.0 eV — a typical limitation of standard GGA-based DFT calculations.

In our previous work [14], we employed the DFT-LDA approach with semiempirical Hubbard U corrections ($U = 5.0$ eV for Si $4d$ states and $U = 4.8$ eV for C $2p$ states) to improve the accuracy of band gap predictions. Our first-principles calculations yielded direct and indirect band gap values of 5.2 eV and 3.3 eV, respectively, for the hexagonal (wurtzite) SiC structure. These results confirm that SiC is an indirect band gap semiconductor, and the calculated indirect gap is in excellent agreement with the experimentally reported value of 3.33 eV [31].

This part of the study examines how aluminum (Al) incorporation modifies the electronic structure of single-walled (6,0) silicon carbide nanotubes (SWSiCNTs), based on density functional theory (DFT) calculations. For the undoped nanotube, the optimized structure exhibits a Si–C bond length of approximately 1.88 Å and an average tube radius close to 3.11 Å, confirming its structural stability and geometric symmetry. When a silicon atom is replaced by an Al dopant, pronounced alterations in the electronic characteristics appear, most notably in the spin-polarized states. Within the LSDA spin framework, the electronic band structures for both spin-up and spin-down channels were systematically examined to reveal these modifications.

When aluminum is introduced into the SiC lattice by replacing a silicon atom, impurity states emerge near the Fermi level, causing a notable reconfiguration of the electronic band structure. The spin-up channel retains semiconducting features but with a significantly reduced band gap of around 1.3 eV, while the spin-down channel exhibits metallic behavior as its band gap completely collapses. This spin-dependent asymmetry marks the onset of half-metallicity, a highly desirable property for spintronic technologies because it supports conduction that is fully polarized with respect to electron spin.

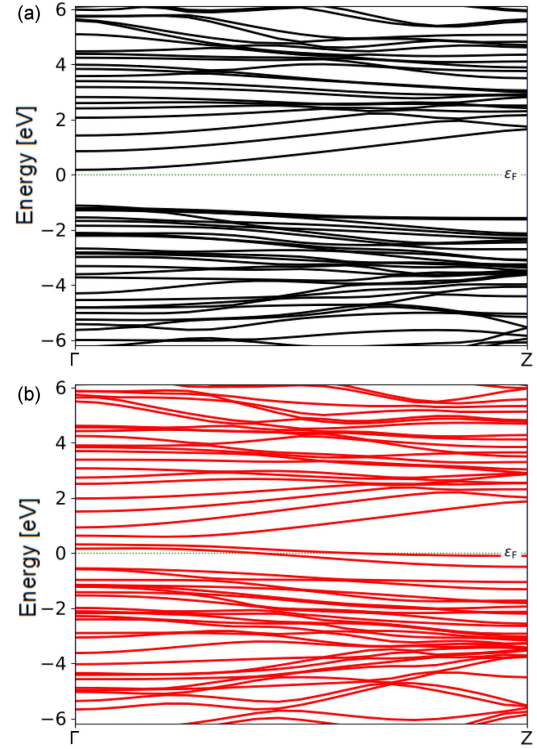


Fig. 1. The calculated spin-up (black, panel a) and spin-down (red, panel b) band structures for Al-doped (6,0) SWSiCNT systems.

The electronic characteristics of the Al-doped (6,0) single-walled silicon carbide nanotube (SWSiCNT) are further elucidated by analyzing the spin-resolved band structures and total density of states (TDOS). To further validate this, the spin-polarized band structures are shown in Fig. 1. The energy bands are plotted along the high-symmetry points from Γ to Z in the Brillouin zone. The position of the Fermi level (dashed line) indicates the electronic behavior of the system, which is crucial for understanding its conductive properties. In Fig. 1a, the spin-up (black) channel is shown, while the spin-down (red) channel is depicted in Fig. 1b. A band gap of ≈ 1.3 eV observed in the spin-up configuration confirms the semiconducting nature of this channel. In contrast, the spin-down channel exhibits metallic behavior, with several bands crossing the Fermi level. This spin-dependent band structure is consistent with the TDOS results and reinforces the half-metallic behavior of the Al-doped SiC nanotube. Such a spin-resolved electronic structure ensures that only electrons with a specific spin orientation contribute to electrical conduction, which is critical for the performance of spintronic devices [32].

The differences between spin-up and spin-down bands highlight the spin polarization effects caused by doping, which are important for analyzing the magnetic and spintronic characteristics of the system.

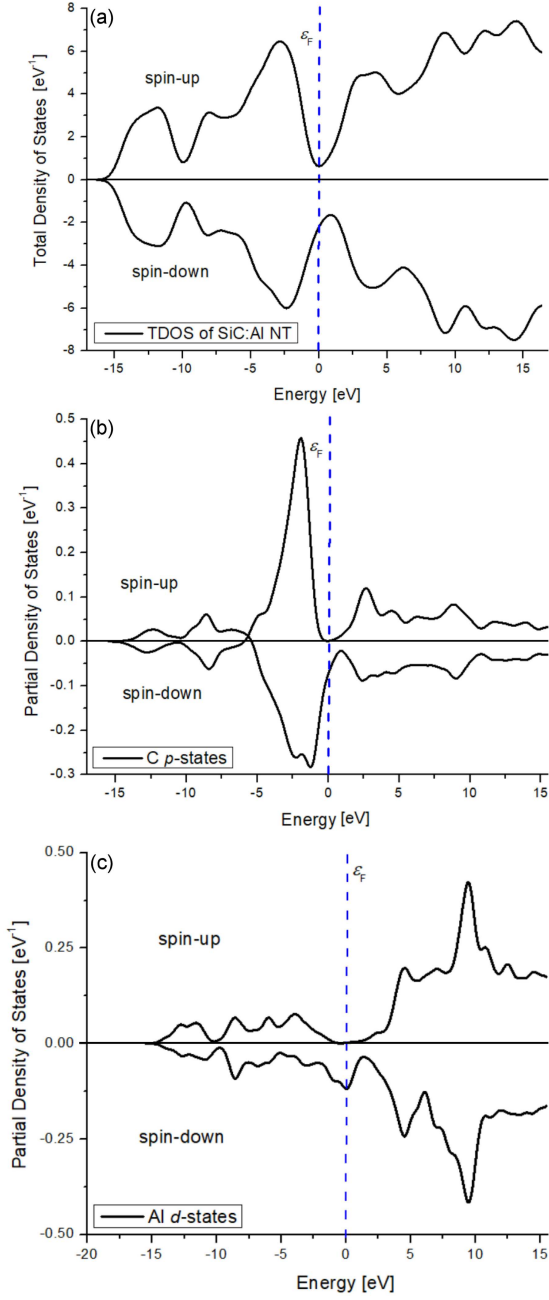


Fig. 2. The calculated total and partial DOS diagrams for Al-doped SWSiCNT.

Figure 2 presents the calculated total and partial density of states (DOS) for the Al-doped single-walled silicon carbide nanotube (SWSiCNT). The Fermi energy level (ϵ_F) is represented by a vertical dashed blue line at 0 eV, which distinguishes occupied states from unoccupied ones at absolute zero temperature. The upper section of the plot corresponds to spin-up states, while the lower section shows spin-down states. The plots clearly demonstrate the spin-resolved contributions of different orbitals to the electronic structure. In particular, the partial DOS reveals that the $3d$ orbitals of the aluminum atom contribute significantly to the valence

band region, confirming their active role in the electronic properties of the system. The spin-up and spin-down components illustrate the spin polarization effects in the material. The carbon p states are also shown, highlighting their dominant contribution near the Fermi level. This comprehensive DOS analysis supports our correction in the paper, where we emphasize the role of Al $3d$ orbitals while excluding any significant involvement of $4d$ orbitals.

A significant asymmetry between the two spin channels is observed, i.e., the spin-up channel maintains a clear band gap at the Fermi level, demonstrating semiconducting behavior, whereas the spin-down channel exhibits a finite density of states that crosses the Fermi level, signifying metallic conductivity. This spin-dependent divergence is characteristic of half-metallic behavior, where one spin orientation conducts like a metal while the other behaves like a semiconductor. This feature is advantageous for spintronic applications, enabling a fully spin-polarized current. The prominent peaks near the Fermi level result from hybridized states formed by the p orbitals of C and the d orbitals of Al, emphasizing the role of orbital interactions in reshaping the electronic structure.

Together, the TDOS and spin-resolved band structure analyses indicate that substituting silicon with aluminum in the SiC nanotube lattice introduces spin asymmetry and induces half-metallic behavior. This is primarily driven by the hybridization between the $2p$ orbitals of carbon and the $3d$ orbitals of aluminum, significantly modifying the local electronic environment around the dopant site. The resulting spin polarization and gap opening in one spin channel make the Al-doped SWSiCNT a promising candidate for use in nanoscale spintronic devices, such as spin filters, spin valves, and magnetic tunnel junctions.

Partial density of states (PDOS) calculations reveal that the electronic states near the Fermi level predominantly originate from the $2p$ orbitals of carbon and the $3d$ orbitals of aluminum. This hybridization is pivotal in the formation of the magnetic moment and the electronic transport properties of the doped system.

In the Al-doped SiC nanotube system, the spin-down band gap is significantly reduced to zero, resulting in metallic behavior due to the crossing of energy bands at the Fermi level near the Γ point of the Brillouin zone. This gap closure enhances the density of states near the Fermi level, thereby improving the electrical conductivity of the Al-doped SiC nanotube. Our calculations show that the electronic states near the Fermi level are mainly contributed by the $3d$ orbitals of aluminum, indicating strong hybridization between the carbon $2p$ orbitals and the aluminum $3d$ orbitals. This orbital interaction plays a crucial role in altering the electronic structure and magnetic properties, driving the transition to a half-metallic state with spin-polarized conduction.

3.2. Magnetic characteristics of SWSiC:Al nanotubes

The Mulliken population analysis of the Al-doped (6,0) SiC nanotube indicates a net spin magnetic moment of $\approx 1.0 \mu_B$, which is attributed to the spin polarization induced by replacing a silicon atom with an aluminum dopant. The spin density distribution reveals that the magnetic moments are primarily localized around the Al dopant site, with significant contributions from nearby carbon atoms that exhibit positive spin polarization. These carbon atoms exhibit enhanced magnetic behavior due to their proximity and electronic interaction with the Al dopant.

In contrast, the Al dopant itself contributes a negative spin magnetic moment, suggesting an antiferromagnetic coupling between the Al atom and its neighboring atoms. This negative moment is partially compensated by silicon atoms in the vicinity, which also exhibit small to moderate negative spin moments. As we move further from the dopant site, the spin polarization weakens, and atomic moments approach zero, indicating a diminishing magnetic influence.

Further analysis of the orbital-resolved Mulliken population provides additional insight into the origins of the magnetism in this system. Silicon atoms primarily exhibit spin polarization in their $3p$ orbitals, with values ranging between 0.6 and 0.7 electrons, while the contribution from their $3s$ orbitals is slightly lower. Minor contributions from silicon d -like orbitals suggest a modest degree of orbital hybridization. In contrast, carbon atoms exhibit strong spin polarization, primarily in their $2p$ orbitals, with smaller contributions from $2s$ orbitals and occasional d -like states, indicating a localized and directional magnetic nature.

The aluminum atom shows significant spin polarization in its $3p$ orbitals, which plays a central role in the system's magnetic behavior. Additionally, smaller spin contributions are observed in its $3s$ and d -like orbitals. The strong hybridization between the Al $3p$ and C $2p$ orbitals is responsible for the induced magnetic moment, playing a crucial role in determining the overall electronic and magnetic properties of the doped SiCNT.

Moreover, the presence of spin polarization in the d -like orbitals throughout the structure indicates that orbital hybridization beyond the basic s and p states contributes to the system's magnetic properties. The total atomic spin magnetic moment arises from the sum of these orbital contributions, confirming the antiferromagnetic nature of the Al-doped SiC nanotube, which suggests its potential applications in spintronic devices.

Figure 3 shows the distribution of spin polarization in the Al-doped (6,0) single-walled silicon carbide (SiC) nanotube. The green arrows represent the direction and magnitude of the local magnetic

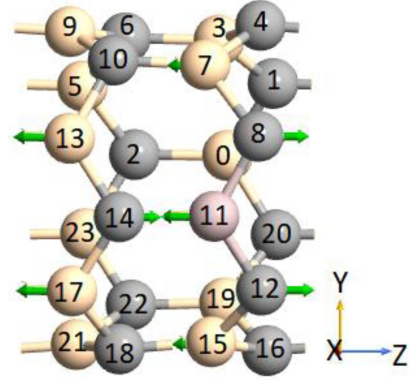


Fig. 3. Spin polarization in Al-doped SiC nanotubes. The green arrows indicate the local magnetic moments. Gray, beige, and pink spheres represent carbon, silicon, and aluminum atoms, respectively.

moments for each atom. Substituting a silicon atom with an aluminum atom in the center of the nanotube induces a distinctive magnetic response in the surrounding atomic lattice.

As illustrated, the C atoms closest to the Al dopant exhibit strong spin polarization, with the spin directions predominantly aligned in one orientation, indicating significant positive magnetic moments. Conversely, the aluminum dopant itself exhibits a negative spin magnetic moment, with the spin vector aligned opposite to that of the surrounding carbon atoms, suggesting an antiferromagnetic interaction between them.

Silicon atoms that are further from the dopant site also show smaller, oppositely aligned spin moments, further confirming the antiferromagnetic ordering across the entire structure. The symmetry and alignment of the spin vectors across the nanotube confirm that the doping process disrupts spin degeneracy, leading to a net spin polarization concentrated around the dopant site.

This overall spin configuration validates the antiferromagnetic ground state of the Al-doped SiC nanotube, which is in agreement with the Mulliken population analysis and total energy comparisons conducted earlier in the study.

The bar chart in Fig. 4 presents the spin magnetic moment distribution for each atom in the Al-doped (6,0) SiC nanotube, as computed using DFT and Mulliken population analysis. Each bar represents a single atom, labeled by its index along the x -axis. The vertical axis corresponds to the magnetic moment in units of Bohr magneton [μ_B]. The color coding reflects the atomic species:

- Gray bars (C atoms)

Many carbon atoms exhibit significant positive spin moments, especially those directly bonded to the Al dopant. These atoms are the primary contributors to the total magnetic moment of the system.

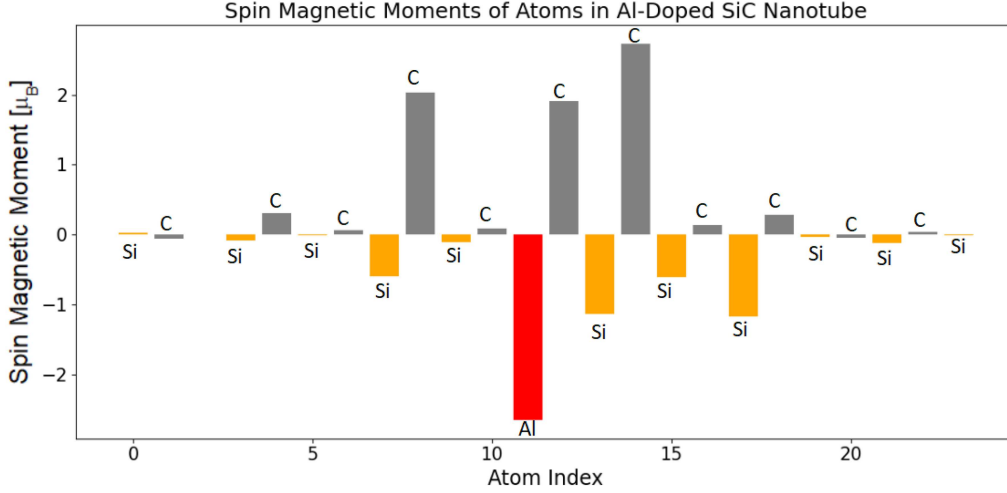


Fig. 4. Spin magnetic moments for individual atoms in the Al-doped (6,0) SiC nanotube.

- **Orange bars (Si atoms)**

Most silicon atoms show small or moderate negative spin moments, indicating antiferromagnetic alignment with the positively polarized carbon atoms.

- **Red bar (Al atom)**

The Al dopant shows a large negative magnetic moment ($\sim -2.64 \mu_B$), which is consistent with its role in inducing strong spin polarization and participating in antiferromagnetic coupling.

The plot shows strong positive spin polarization on carbon atoms near the Al dopant and significant negative polarization on the Al and nearby Si atoms, confirming antiferromagnetic coupling and localized spin distribution.

The substitution of a single Si atom with an Al atom significantly modifies the local spin environment, leading to pronounced spin polarization effects near the dopant site. The Al atom (shown as a red bar) exhibits a large negative spin magnetic moment of $\approx -2.64 \mu_B$, serving as the dominant contributor to the overall magnetism of the system. This strong local moment originates from unpaired electrons in the Al $3p$ orbitals and their hybridization with surrounding orbitals. Notably, the nearest-neighbor carbon atoms display strong positive spin polarization (gray bars), while the adjacent silicon atoms generally exhibit negative spin moments (orange bars), indicating a ferrimagnetic-like coupling between the dopant and host atoms. The spin polarization weakens progressively with increasing distance from the Al site, suggesting that the magnetic perturbation is highly localized. Interestingly, the distribution of spin magnetic moments around the Al dopant is not perfectly symmetric, even though the substitution was performed at a site intended to preserve the structural symmetry of the (6,0) nanotube. This apparent asymmetry can

be attributed to local structural relaxation caused by the size and electronegativity mismatch between Al and Si, which leads to slightly different bonding geometries for neighboring atoms. Additionally, asymmetric charge redistribution and orbital hybridization effects may contribute to the observed non-uniform spin density.

These results highlight the localized and dopant-driven magnetic character of the Al-doped SiCNT system and demonstrate that single-atom substitution can effectively induce spin polarization, which may have potential implications for nanoscale spintronic devices.

Table I summarizes the essential electronic and magnetic properties of Al-doped (6,0) single-walled silicon carbide nanotubes (SWSiCNTs), derived from first-principles calculations. The results confirm the emergence of half-metallic behavior, driven by modifications in the spin-resolved band structure and strong spin polarization localized around the Al dopant. This behavior, coupled with the energetically favorable antiferromagnetic (AFM) ground state, highlights the potential of the material for use in spintronic devices.

The total spin distribution analysis reveals that the magnetic properties of the system are localized predominantly around the Al dopant and its immediate carbon neighbors. The total spin magnetic moment is $\approx 1.0 \mu_B$, indicating that the system possesses a net magnetic moment due to an incomplete cancellation between the spin-up and spin-down electron populations. This finding supports the earlier identification of half-metallic and antiferromagnetic properties in the electronic structure, further emphasizing the suitability of this material for spintronic applications.

To determine the magnetic ground state of the system, total energy calculations were performed for both ferromagnetic (FM) and antiferromagnetic (AFM) configurations. The total energy for the FM

Summary of electronic and magnetic properties of Al-doped (6,0) SWSiCNT.

TABLE I

Property	Value / Description
structure type	single-walled (6,0) SiC nanotube (SWSiCNT)
bond length (Si-C)	$\sim 1.88 \text{ \AA}$
tube radius	$\sim 3.11 \text{ \AA}$
doping type	substitutional doping of Si atom by Al
exchange-correlation functional	LSDA + Hubbard U correction (LSDA+ U)
corrected band gaps (bulk SiC)	5.2 eV (direct), 3.3 eV (indirect)
band gap (spin-up channel)	$\sim 1.3 \text{ eV}$ (semiconducting)
band gap (spin-down channel)	0 eV (metallic)
electronic behavior	half-metallic (metallic in one spin channel, semiconducting in the other)
Fermi level contribution	dominated by hybridized Al $4d$ and C $2p$ orbitals
density of states (DOS)	spin-asymmetric; metallic behavior in spin-down channel
spin magnetic moment (total)	$\sim 1.0 \mu_B$
magnetization origin	strong positive spin moments from C atoms near Al dopant; negative moment on Al atom
spin moment of Al dopant	$\sim -2.64 \mu_B$ (negative value)
magnetic coupling	antiferromagnetic (AFM) alignment between Al and neighboring Si, C atoms
magnetic ground state	AFM more stable than FM by $\sim 21.0452 \text{ eV}$
orbital contributions (dominant)	for C — $2p$ orbitals; for Si — $3p$ orbitals; for Al — $3p$ and $3d$ orbitals
spin localization	strongly localized around Al dopant and adjacent carbon atoms
potential applications	spin filters, magnetic memory, spin injectors, nano-optoelectronics

state was found to be -3891.47261 eV , while the AFM state exhibited a lower total energy equal to -3912.51781 eV . This energy difference indicates that the AFM configuration is more stable, confirming it as the ground state for the Al-doped (6,0) SWSiCNT system.

It is important to clarify that although our system exhibits an antiparallel alignment of magnetic moments with a net total magnetic moment ($\sim 1.0 \mu_B$), which may suggest ferrimagnetic behavior by bulk material standards, the total energy calculations confirm the AFM configuration as the ground state. This discrepancy arises due to the localized nature of spin polarization induced by Al doping in the one-dimensional nanotube structure. Unlike bulk materials, where antiferromagnetism implies zero net magnetic moment, low-dimensional doped systems can display unbalanced antiparallel moments leading to a non-zero total moment. Therefore, we describe the magnetic ground state as antiferromagnetic with an unbalanced magnetic moment resulting from doping-induced local effects.

These findings reinforce the potential of Al-doped SiC nanotubes for next-generation spintronic and antiferromagnetic devices. The unique magnetic behavior and half-metallic characteristics, combined with the material's structural stability, make these nanotubes promising candidates for various nanoscale applications, including spin filters, memory components, and other elements in nano-optoelectronic technologies.

4. Conclusions

In this work, we performed a detailed first-principles study of the electronic and magnetic properties of aluminum-doped single-walled (6,0) silicon carbide nanotubes (SWSiCNTs) using density functional theory (DFT). The findings reveal that the substitution of Si atoms with aluminum significantly alters the electronic structure, resulting in spin-dependent modifications and leading to half-metallic behavior.

The spin-polarized charge density and Mulliken population analyses indicate a total magnetic moment of approximately $1.0 \mu_B$, mainly originating from C atoms directly bonded to the Al dopant. An antiferromagnetic interaction is observed between the Al atom and its neighboring Si atoms, which contributes to the overall magnetic properties. Additionally, total energy comparisons between ferromagnetic (FM) and antiferromagnetic (AFM) configurations show that the AFM configuration is energetically more stable, confirming its position as the ground state for the system.

In conclusion, the Al-doped (6,0) SWSiCNTs exhibit desirable characteristics, including tunable half-metallicity, strong spin polarization, and a stable antiferromagnetic ground state. These properties make the material a promising candidate for next-generation spintronic devices, such as spin filters, spin injectors, and antiferromagnetic memory components.

References

- [1] W. Zhang, F. Zhang, Z. Zhang, S. Lu, Y. Yang, *Sci. China Phys. Mech.* **53**, 1582 (2010).
- [2] R. Madar, *Nature* **430**, 974 (2004).
- [3] K.M. Alam, A.K. Ray, *Phys. Rev. B* **77**, 035436 (2008).
- [4] B. Baumeier, P. Krüger, J. Pollmann, *Phys. Rev. B* **76**, 085407 (2007).
- [5] J.S. Ponraj, S.C. Dhanabalan, G. Attolini, G. Salviati, *Crit. Rev. Solid State Mater. Sci.* **41**, 430 (2016).
- [6] E. Santos, A. Ayuela, D. Sanchez-Portal, *New J. Phys.* **12**, 053012 (2010).
- [7] J.-X. Zhao, Y.-H. Ding, *J. Phys. Chem. C* **112**, 2558 (2008).
- [8] H. Heidarzadeh, *Opt. Quant. Electron.* **51**, 32 (2019).
- [9] A.T. Mulatu, K.N. Nigussa, L.D. Deja, *Opt. Mater.* **134**, 113094 (2022).
- [10] C. Vatankehah, H.A. Badehian, *Optik* **237**, 166740 (2021).
- [11] R.Z. Ibaeva, V.N. Jafarova, V.I. Eminova, I.C. Scurtu, S. Lupu, *J. Nanopart. Res.* **26**, 23 (2024).
- [12] V.N. Jafarova, S.S. Rzayeva, I.C. Scurtu, C. Stanca, N. Acomi, G. Raicu, *Adv. Nat. Sci. Nanosci. Nanotechnol.* **15**, 035012 (2024).
- [13] V.N. Jafarova, V.I. Eminova, M.A. Musaev, I.C. Scurtu, *Technium* **26**, 1 (2025).
- [14] N.T. Tien, P.T.B. Thao, V.N. Jafarova, D.D. Roy, *Silicon* **1**, (2024).
- [15] S. Rzayeva, V.N. Jafarova, D.D. Roy, *Mater. Sci. Semicond. Process.* **197**, 109702 (2025).
- [16] S. Rzayeva, V.N. Jafarova, *Turkish Comput. Theor. Chem.* **9**, 112 (2025).
- [17] S. Rzayeva, V.N. Jafarova, *J. Polytech.* **28**, 947 (2025).
- [18] A.Q. Wu, Q.G. Song, L. Yang, *Adv. Mater. Res.* **510**, 747 (2012).
- [19] W. Kohn, L.J. Sham, *Phys. Rev.* **140**, A1133 (1965).
- [20] M. Cococcioni, S. de Gironcoli, *Phys. Rev. B* **71**, 035105 (2005).
- [21] A.V. Sinelnik, A.V. Semenov, *Condens. Matter Phys.* **24**, 23706 (2021).
- [22] Z. Huang, T.-Y. Lü, H.-Q. Wang, J.-C. Zheng, *AIP Adv.* **5**, 097204 (2015).
- [23] C.H. Park, B.H. Cheong, K.H. Lee, K.J. Chang, *Phys. Rev. B* **49**, 4485 (1994).
- [24] L. Sun, Y. Li, Z. Li, Q. Li, Z. Zhou, Z. Chen, J. Yang, J.G. Hou, *J. Chem. Phys.* **129**, 174114 (2008).
- [25] G. Alfieri, T. Kimoto, *Appl. Phys. Lett.* **97**, 043108 (2010).
- [26] P. Lou, J.Y. Lee, *J. Phys. Chem. C* **113**, 21213 (2009).
- [27] E. Bekaroglu, M. Topsakal, S. Cahangirov, S. Ciraci, *Phys. Rev. B* **81**, 075433 (2010).
- [28] M. Zhao, Y. Xia, F. Li, R.Q. Zhang, S.-T. Lee, *Phys. Rev. B* **71**, 085312 (2005).
- [29] A.T. Mulatu, K.N. Nigussa, L.D. Daja, *Materialia* **20**, 101257 (2021).
- [30] E.V. Larina, V.I. Chmyrev, V.M. Skorikov, P.N. D'yachkov, D.V. Makaev, *Inorg. Mater.* **44**, 823 (2008).
- [31] G.L. Harris, *Properties of Silicon Carbide*, INSPEC, London (1995).
- [32] J. Patyk, R. Rich, M. Wieligor, W. Żerda, *Acta Phys. Pol. A* **118**, 480 (2010).